

Tailored Interphases Construction for Enhanced Si Anode and Ni-Rich Cathode Performance in Lithium-Ion Batteries

Yuxiang Huang¹, Yuchen Ji¹, Guorui Zheng²*, Hongbin Cao¹, Haoyu Xue¹, Xiangming Yao¹, Lu Wang¹, Shiming Chen¹, Zuwei Yin³, Feng Pan¹* & Luyi Yang¹*

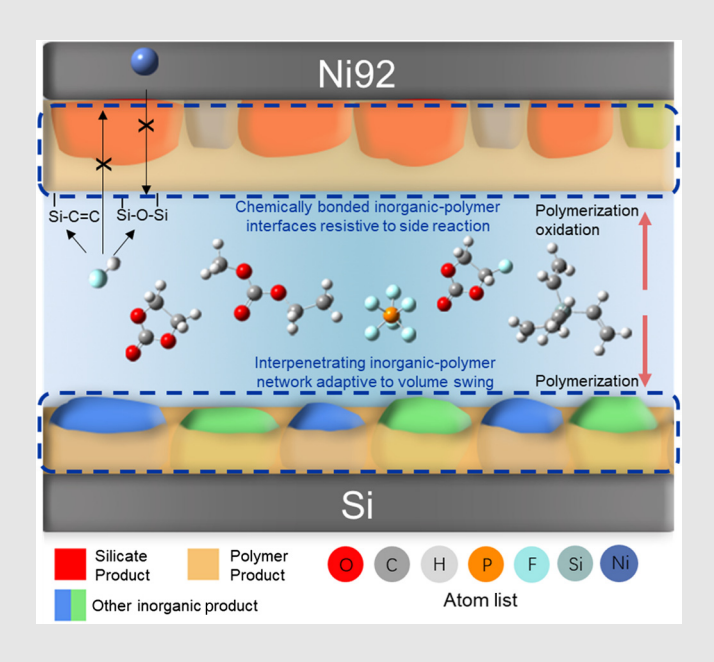
¹School of Advanced Materials, Peking University Shenzhen Graduate School, Shenzhen 518055, ²Institute of Materials Research (IMR), Tsinghua Shenzhen International Graduate School, Tsinghua University, Shenzhen 518055, ³College of Energy, Xiamen University, Xiamen 361005

*Corresponding authors: zhengguorui1991@163.com; panfeng@pkusz.edu.cn; yangly@pkusz.edu.cn; 'Y. Huang and Y. Ji contributed equally to this work.

Cite this: *CCS Chem.* **2025**, 7, 429-439 **DOI:** 10.31635/ccschem.024.202404120

As promising candidates for high-energy-density lithium-ion batteries, both silicon (Si) anodes and nickel-rich cathodes face significant challenges due to structural instability arising from interphases. In this study, we introduced tetravinylsilane (TVSi) as a multifunctional electrolyte additive to engineer tailored interphases simultaneously on Si anode and $LiNi_{0.92}Mn_{0.05}Co_{0.03}O_2$ cathode, thereby enhancing their electrochemical performance. On one front, TVSi underwent polymerization, leading to the formation of a composite solid electrolyte interphase (SEI) with an interpenetrating network structure on the Si surface. This SEI effectively accommodated volume changes during cycling, which inhibited SEI growth, hence, preserving the battery capacity. On the other hand, the TVSi-induced cathode electrolyte interphase (CEI) exhibited a dense structure comprising a chemically bonded silicate-silane polymer. This CEI effectively mitigated transition metal dissolution by scavenging hydrofluoric acid (HF) and reduced irreversible phase transitions by minimizing side reactions. As a result of the enhanced interfacial stability achieved on both electrodes, TVSi enabled improved performance in full cells fabricated with a LiNi_{0.92}Mn_{0.05}Co_{0.03}O₂ cathode paired with a Si

anode. This multifunctional additive strategy offers a novel perspective on additive design for highenergy-density lithium-ion batteries, showcasing its potential for advancing battery technology.



Keywords: electrolyte additive, solid electrolyte interphase, cathode electrolyte interphase, in situ interface characterization, lithium-ion battery

DOI: 10.31635/ccschem.024.202404120 **Citation:** *CCS Chem.* **2025**, 7, 429-439



Introduction

The increasing demand for portable energy storage has promoted the development of lithium-ion batteries toward cheaper price, higher energy density, and longer lifespan. In this respect, silicon (Si) has become a promising candidate for anode due to its high theoretical capacity, low working plateau, and abundant resources. For the cathode candidates, high-nickel (Ni) layered oxide $\text{LiNi}_x \text{Mn}_y \text{Co}_z \text{O}_2$ (x + y + z = 1, x > 0.9) materials stand out for the higher specific capacity at the same cutoff voltage. Therefore, pairing Ni-rich cathode and Si anode is likely to meet the commercial requirement for high-energy-density lithium-ion batteries.

However, toward their commercialization, a series of issues remain unsolved. For the Si anode, the main challenge is the instability of the solid electrolyte interphase (SEI) caused by the continuous Si volume swing.^{5,6} The expansion and shrink can damage the SEI and expose the Si particle surface to the electrolyte, resulting in continuous electrolyte consumption and SEI growth.⁷

Fluorinated carbonates such as fluoroethylene carbonate (FEC) are frequently reported as an effective anode additive,8-11 owing to their ability to construct an inorganic LiF-rich SEI with higher chemical stability and hardness. 12,13 However, merely increasing the amount of hard inorganic products is insufficient to form a resilient SEI. As for Ni-rich cathodes, the thermal decomposition or electrochemical oxidation of FEC and lithium hexafluorophosphate (LiPF₆) salt can generate various acids (e.g. HF), especially at high voltages, 14-17 which is commonly reported to trigger the transition metal (TM) dissolution, leading to structural degradation of Ni-rich cathode materials. 18,19 Therefore, constructing interphases with superior mechanical and chemical properties on both Si anode and Ni-rich cathode is essential to mitigate the above interphase-originated issues.^{20,21} One of the key pathways is to modify the interphases in-situ via multifunctional electrolyte additive engineering, so that the stable cathode electrolyte interphase (CEI) and SEI can be simultaneously constructed on cathode and anode, respectively.

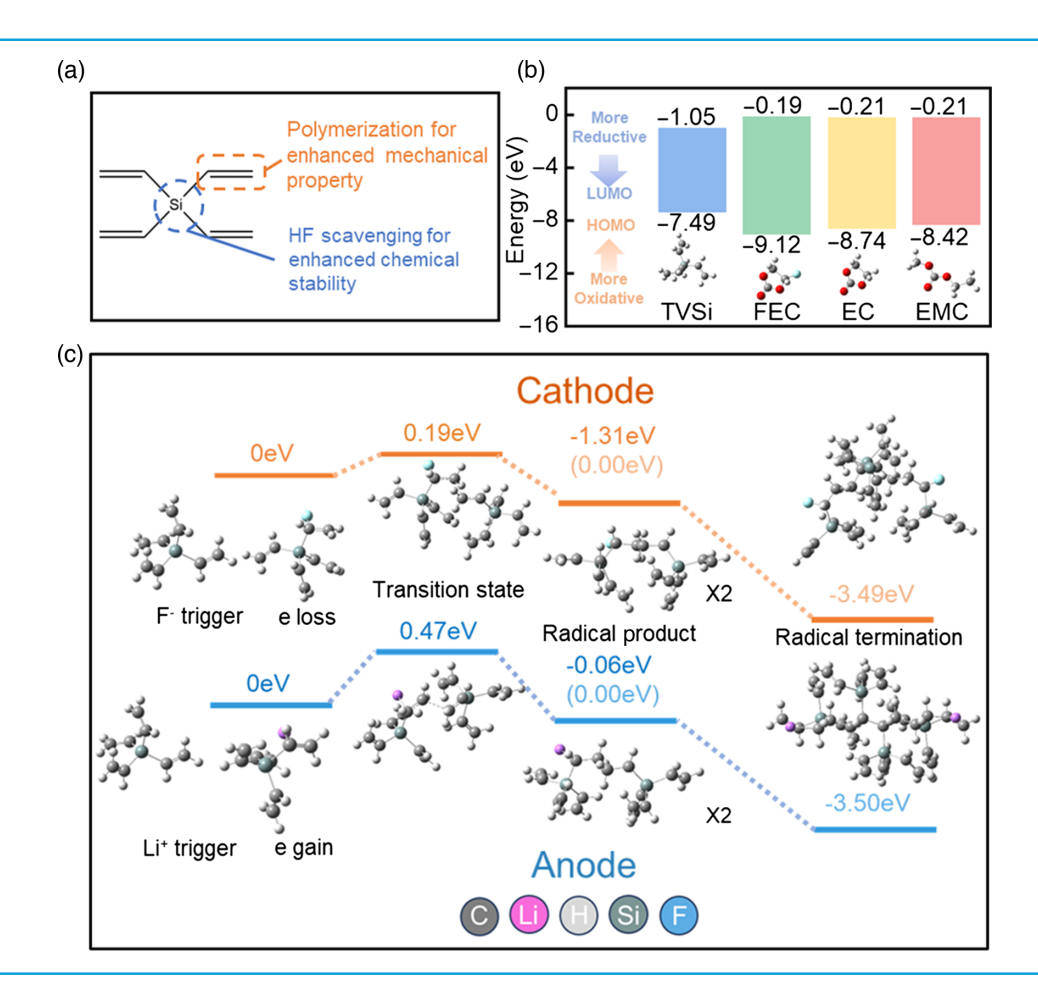


Figure 1 (a) Molecular structural design strategy for TVSi additive. (b) The LUMO and HOMO energy levels of TVSi, FEC, EC, and EMC. (c) Proposed polymerization processes of TVSi at cathode and anode. LUMO, lowest unoccupied molecular orbital; HOMO, highest occupied molecular orbital; FEC, fluoroethylene carbonate; EC, ethylene carbonate; EMC, ethyl methyl carbonate.

DOI: 10.31635/ccschem.024.202404120 **Citation:** *CCS Chem.* **2025**, 7, 429-439



Considering the key origins of interfacial instability on Si-based anodes and Ni-rich cathodes are different, a wealth of molecular properties (e.g. decomposition voltages and decomposition products) should be taken into consideration for choosing additives. On the surface of Si anodes, the SEI should exhibit a structure characterized by flexibility and adaptability, complemented by appropriate mechanical strength to accommodate volumetric changes. In contrast, for the cathode surface, a structurally rigid and dense configuration is essential for the CEI to effectively prevent electrolyte penetration and enhance interfacial stability.

Herein, tetravinylsilane (TVSi) was proposed as a promising additive due to its unique molecular structure (Figure 1a). With four carbon-carbon double bonds and a Si-based structure, we expected TVSi to form crosslinked polymeric species.^{22,23} Additionally, it has been reported that silanes serve as HF scavengers in the electrolyte, protecting the phase of Ni-rich cathodes. 24,25 In this work, 1 wt % TVSi was introduced into a commercial electrolyte [1 M LiPF₆ in ethylene carbonate:ethyl methyl carbonate (EC:EMC) = 3:7 vol % with 10 wt % FEC] for high-performance nano-Si anode and LiNi_{0.92}Mn_{0.05}Co_{0.03}O₂ (Ni92) cathode. Through comprehensive characterizations coupled with theoretical calculations, the protection mechanisms of Si anodes and Ni-rich cathodes were revealed. On the surface of the Si anode, the polymerization process formed an SEI with a distinctive interpenetrating network structure on Si, featured by rigid inorganic species embedded in a flexible silane polymer framework. This structure enhanced the modulus and uniformity of the SEI, enabling it to maintain its integrity during the Si volume swing and further, restricted the SEI growth. On the surface of Ni92, a dense CEI layer featured by covalently bonding organic polymers with inorganic substances structure was generated, which impeded the electrolyte penetration, lessened the interface side reactions, and alleviated the irreversible phase transformation. Through the construction of chemically and mechanically stable interphases on both sides of the electrodes, the proposed multifunctional additive effectively improved the performance of the full cell.

Experimental Methods

Electrolytes and electrode preparation

The baseline electrolyte (BE) comprised 1 M LiPF $_6$ in EC:EMC = 3:7 vol % with 10 wt % FEC. The experimental group contained an extra 1 wt % TVSi. The anode consisted of Si, acetylene black (AB), and polyacrylic acid (PAA) in 3:1:1 (wt %), applied to copper foil. For the cathode, LiNi $_{0.92}$ Mn $_{0.05}$ Co $_{0.03}$ O $_2$, AB, and polyvinylidene fluoride (PVDF) were mixed at an 8:1:1 weight ratio and coated onto aluminum foil.

Cell assembly and electrochemical measurement

All the cells in this work were assembled, 20 mm diameter, 3.2 mm height (CR2032) coin cells. The coin cells were initially activated and continuously charged and discharged (Si: 0.2C = 840 mA/g; Ni92 1C = 200 mA/g) under galvanostatic control at 25 °C or 45 °C. All the electrochemical measurements were carried out by the Neware battery test system (Neware Technology Ltd., Shenzhen, China). For the electrochemical impedance spectroscopy (EIS) test, the cells were monitored in the frequency range from 1 MHz to 0.01 Hz.

Characterization

Fourier transform infrared spectroscopy (FTIR, Thermo Fisher Scientific (China) Co., Ltd., Shanghai, China) was utilized to observe variations in electrolyte components. Atomic force microscopy (AFM, (Beijing) Scientific Technology Co., Ltd., Beijing, China), X-ray photoelectron spectroscopy (XPS, Thermo Fisher Scientific (China) Co., Ltd., Shanghai, China), and time of flight secondary ion mass spectrometry (TOFSIMS, ULVAC-PHI (Nanjing) Instrument Ltd., Nanjing, China) were used for analyzing the chemistry and properties of SEI and CEI. Electrochemical quartz crystal microbalance (EQCM, Ametek Commercial Enterprise (Shanghai) Co., Ltd., Shanghai, China), inductively coupled plasma atomic emission spectroscopy (ICP-AES, Hori Trading (Shanghai) Co., Ltd, Shanghai, China), and ultraviolet-visible (UV-vis, Shimadzu (China) Co., Ltd, Shanghai, China) spectroscopy were utilized for monitoring TM variation. Scanning electron microscopy (SEM, Carl Zeiss (Shanghai) Co., Ltd., Shanghai, China) and transmission electron microscopy (TEM, JEOL (Beijing) Co., Ltd., Beijing, China) were used to observe the microstructure of the materials.

Computational methods

Density functional theory (DFT) was used to investigate the reaction mechanisms, analyze molecular orbital energies, and simulate infrared vibrations. Molecular dynamics (MDs) simulation was utilized to explore the behavior of electrolyte components. More detailed information can be found in the Supporting Information.

Result and Discussion

The film-forming capability of TVSi is initially evaluated through theoretical calculations. First, the lowest unoccupied molecular orbital (LUMO) and the highest occupied molecular orbital (HOMO) levels of the electrolyte solvents and TVSi were calculated to verify the electrochemical redox reaction priority (Figure 1b). Compared

DOI: 10.31635/ccschem.024.202404120 **Citation:** *CCS Chem.* **2025**, 7, 429-439



with other solvents, TVSi exhibited the lowest LUMO energy (-1.05 eV) and the highest HOMO energy (-7.49 eV), indicating that TVSi was the most favorable component for both reduction and oxidation reactions in the electrolyte; hence, served as a suitable sacrificial filmforming agent for both cathodes and anodes. Then to prove the feasibility of TVSi polymerization reaction on electrodes, DFT calculations were carried out (Figure 1c and Supporting Information Figures S1 and S2), showing that TVSi underwent F⁻ and Li⁺ triggered carbon-carbon double bond cleavage reactions on cathode and anode sides, respectively. At the anode, the energy of this reaction transition state was 0.47 eV higher than the reactants, which was a relatively low energy barrier, while the energy of the generated radical products was 0.06 eV lower than the reactants. In practical situations, the presence of additional electrical energy was conducive to overcoming the transition state of the reaction. These radicals eventually underwent a radical termination process with other radicals, resulting in a final energy state that is 3.50 eV lower than the combined energy of the two radicals (e.g., bimolecular termination). Similar results at the cathode prove that both reaction processes are thermodynamically and kinetically favorable. These calculations all suggest that TVSi can polymerize in situ on the surface of the electrodes, forming polymer

electrodes-electrolyte interphase components to protect the anode and cathode.

The galvanostatic cycling performance of Si anodes with a baseline electrolyte (denoted as BE) and 1% TVSi containing electrolyte (denoted as BE + 1%TVSi) was evaluated at room temperature (Figure 2a,b). Both electrolytes deliver similar initial specific capacities at 0.2 C after activation. As shown in Supporting Information Figure S3, with TVSi, the curve exhibited a slightly prolonged plateau during the initial cycle activation, indicating that TVSi decomposed and participated in the formation of the SEI during the initial cycle activation. Thanks to the TVSi additive, the specific capacity retention of the Si anode greatly increased from 30% to 80% after 300 cycles, with 2281 mAh g⁻¹ specific capacity remaining. The working voltage of the TVSi group in the final cycle was maintained at 0.31 V, while the blank declined to 0.24 V with shorter and more pronounced overpotentials. Compared with BE, a superior rate capability was also achieved by BE + 1%TVSi (Supporting Information Figure S4a) owing to the lower impedance (Supporting Information Figure S5). The electrochemical performance improvement was exhibited more remarkably under harsh operating conditions. With a 1% TVSi additive, the capacity retention of the Si anode was maintained at 70% after 150 cycles at 45 °C (Supporting

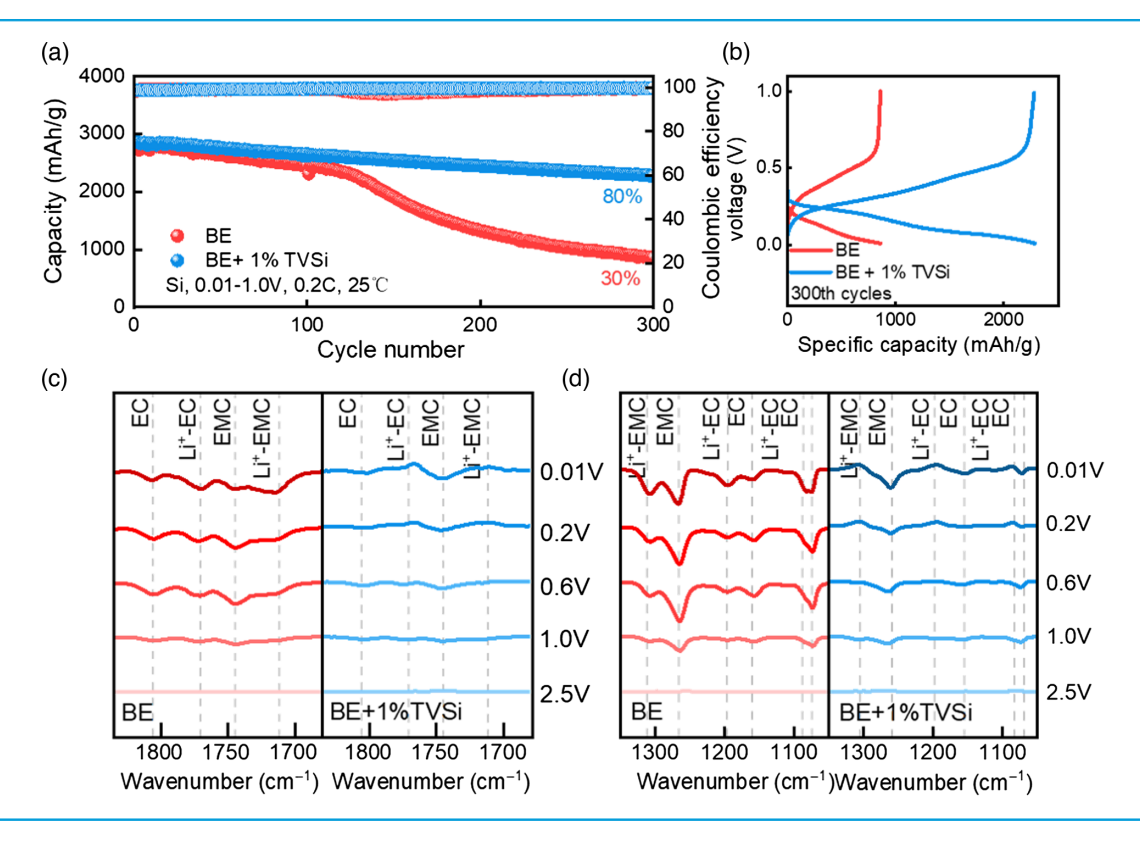


Figure 2 | Electrochemical performance of Si|\Li half cells. (a) Cycle performance at 25 °C, (b) capacity-voltage curve at the 300th cycle. In-situ FTIR measurement on Si surface: (c) In-situ FTIR difference spectra within C=O stretching region on Si with BE (in red) and BE + 1% TVSi (in blue), (d) C-O stretching region. FTIR, Fourier transform infrared spectroscopy.

DOI: 10.31635/ccschem.024.202404120 **Citation:** *CCS Chem.* **2025**, 7, 429-439



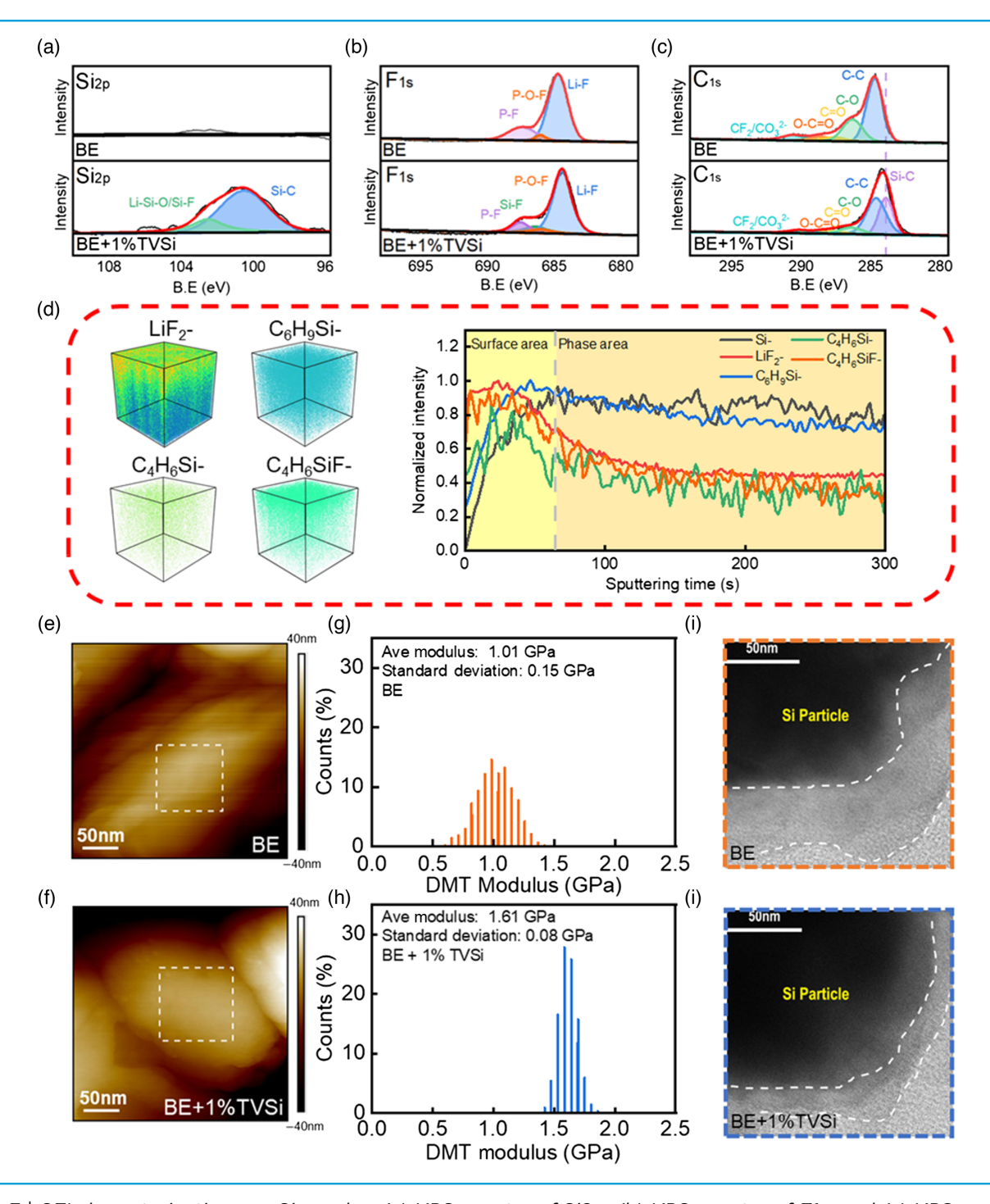


Figure 3 | SEI characterizations on Si anodes. (a) XPS spectra of Si2p, (b) XPS spectra of F1s, and (c) XPS spectra of C1s. (d) TOFSIMS 3D visualization spectra for Si $^-$, LiF $_2$ $^-$, C_6H_9Si $^-$, and C_4H_6Si $^-$ debris with BE + 1% TVSi. AFM images (e, f) of the Si particle with (e) BE and (f) BE + 1% TVSi, and the modulus distribution graphs (g, h) of the SEI derived from them. TEM images of the Si SEI after 200 cycles with (i) BE and (j) BE + 1% TVSi. SEI, solid electrolyte interphase; XPS, X-ray photoelectron spectroscopy; TOFSIMS, time of flight secondary ion mass spectrometry; 3D, three-dimensional; AFM, atomic force microscopy.

Information Figure S4b). In comparison, due to the accelerated side reactions, the capacity of the BE group nearly faded to zero after 150 cycles.

To verify the reduction mechanism of TVSi on the Si anode, the electrolyte environment was initially

examined by MD calculation and FTIR. Differences can be hardly observed in the radial distribution function (RDF) graphs and FTIR spectra between BE and BE + 1% TVSi (Supporting Information Figures S6 and S7), revealing that the addition of TVSi barely influenced the

DOI: 10.31635/ccschem.024.202404120 **Citation:** *CCS Chem.* **2025**, 7, 429-439



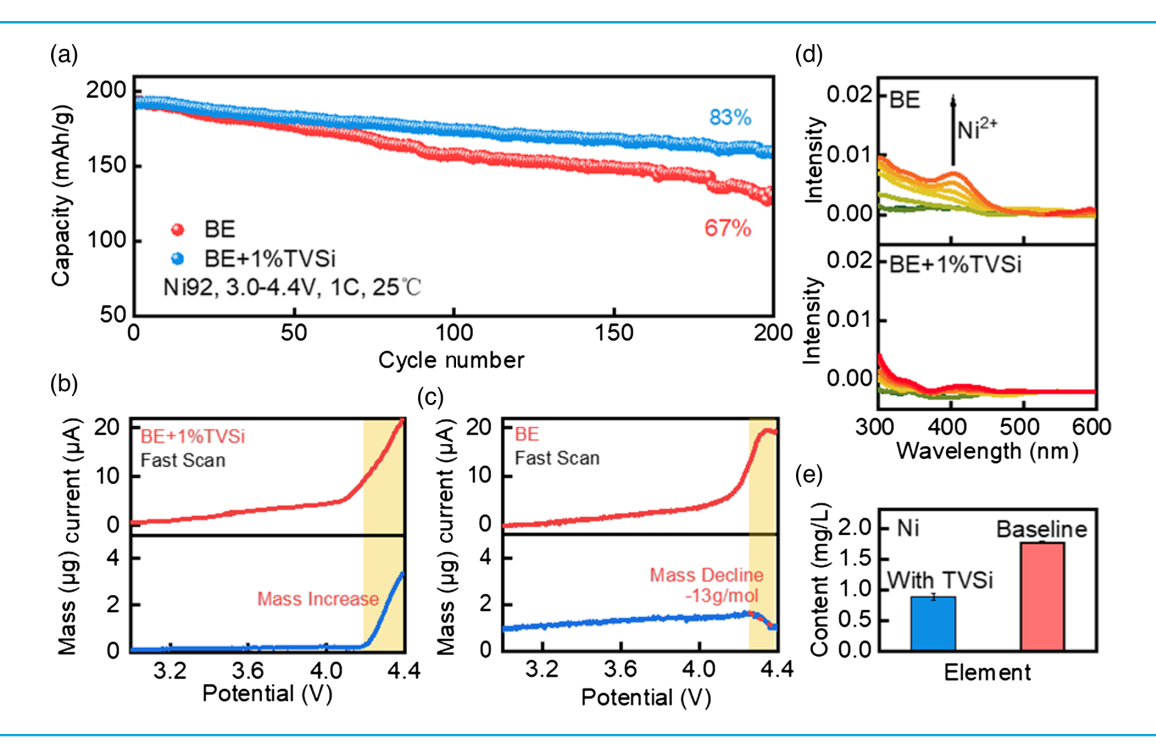


Figure 4 | (a) Cycle performance at 25 °C of Ni92 half cells with the blank electrolyte and 1% TVSi additive electrolyte. EQCM result: (b) the blank electrolyte and (e) 1% TVSi additive electrolyte. (c) In-situ UV-vis result of the blank electrolyte and 1% TVSi additive electrolyte. (d) ICP-AES result of nickel ion content at the lithium metal anode. EQCM, electrochemical quartz crystal microbalance; ICP-AES, inductively coupled plasma atomic emission spectroscopy.

lithium-ion solvation structure. For further study, in-situ FTIR was applied to reveal the interfacial evolution of electrolyte as the SEI formation process at the initial cycle (Figure 2c,d and Supporting Information Figure S8).^{26,27} It should be noted that the FTIR signals recorded at open circuit voltage (2.5 V) were used as baseline; hence, all reverse peaks detected in-situ indicated consumption of specific electrolyte components near the electrode surface. As the potential discharging to a relatively low potential range, the signals presenting EC (1806 cm⁻¹, 1162 cm⁻¹), Li⁺-EC (1770 cm⁻¹, 1196 cm⁻¹), EMC $(1745 \text{ cm}^{-1}, 1265 \text{ cm}^{-1})$ and $\text{Li}^+\text{-EMC}$ $(1713 \text{ cm}^{-1}, 1308 \text{ cm}^{-1})$ exhibited obvious attenuation in BE, indicating the drastic decomposition of organic solvent as the formation of SEI. By contrast, the corresponding decomposition peaks of the above-mentioned solvents were dramatically inhibited in the presence of the TVSi additive. It is believed that the organic components of SEI derived from solvent decomposition are unstable, failing to provide enough chemical stabilities and mechanical properties to accommodate the volume expansion of Si anode.²⁸ Thanks to the decomposition of TVSi prior to the decomposing potential of solvents (Figure 1b), a passivation interphase can be effectively constructed on the surface of Si anode to inhibit the unlimited decompositions of solvents, contributing to the formation of compact and robust SEI.

XPS and TOFSIMs were carried out to investigate the differences in SEI components and structure. For the Si2p

spectra (Figure 3a and Supporting Information Figure S9), two new peaks corresponding to Li-Si-O/Si-F (102.5 eV) and Si-C (100.5 eV) appeared when 1% TVSi was added, while no peaks could be observed in BE.^{29,30} After etching for 40 s, Si-O and Li-Si-O signals began to appear in the BE group (Supporting Information Figure \$10). The above results indicated that the Si-containing species detected on the anode surface originated from the decomposition of TVSi while the in-depth signals were attributed to bulk Si. For BE + 1% TVSi, extra new peaks were noted in F1s spectra at 686.4 eV and a new peak in C1s spectra at 283.6 eV, confirming the existence of Si-F and Si-C bonding, respectively (Figure 3b,c).^{31,32} These XPS peaks demonstrated the existence of silanederived polymer products on the Si surface. TOFSIMS results were in agreement with XPS (Figure 3d), where both silane polymer fragments and fluorides were detected. From the distribution curves, it could be found that the silane relative fragments had similar distribution tendencies as fluorides such as LiF₂⁻. Therefore, it could be speculated that TVSi decomposed simultaneously with FEC on the anode side, forming an inorganic-silane interpenetrating network composite SEI, expected to have improved the modulus distribution and minimized the stress concentration points.

To verify the above speculation, AFM was employed to measure the mechanical property of SEI on Si. To ensure the measurements reflect the SEI on the Si anode surface, the nano-Si particle morphologies were initially detected,

DOI: 10.31635/ccschem.024.202404120 **Citation:** *CCS Chem.* **2025**, 7, 429-439



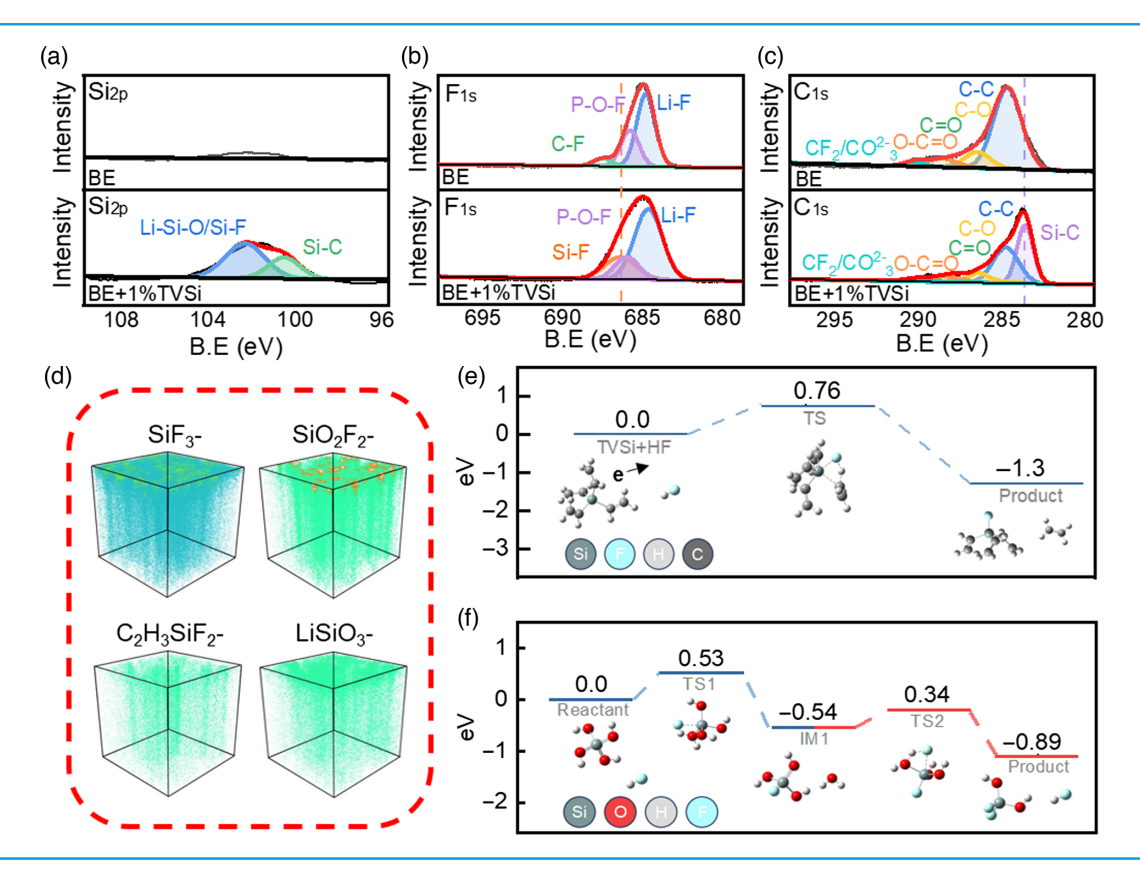


Figure 5 | Characterization of the CEI chemical components and structure of the Ni92 cathode using the blank electrolyte and 1% TVSi additive electrolyte: (a) XPS spectra of Si 2p, (b) XPS spectra of F 1s, (c) XPS spectra of C 1s. (d) TOFSIMS 3D visualization spectra for $LiSiO_3^-$, $SiO_2F_2^-$, SiF_3^- , and $C_2H_3SiF_2^-$ debris with different electrolytes. HF scavenging process of TVSi at the cathode: (e) reaction between TVSi and HF, and (f) reaction between silicate and HF. CEI, cathode electrolyte interphase; XPS, X-ray photoelectron spectroscopy; TOFSIMS, time of flight secondary ion mass spectrometry; 3D, three-dimensional.

and the brightest regions with minimum height variations were chosen to measure the modulus (Figure 3e,f). As shown in Figure 3g,h, the average modulus of the SEI in BE is 1.01 GPa with a standard deviation of 0.15 GPa. In comparison, TVSi addition resulted in a higher average modulus of 1.61 GPa and a lower standard deviation of 0.08 GPa, suggesting a harder and more homogeneous SEI. According to the in-situ FTIR results, with the addition of TVSi, the decomposition of organic solvents was inhibited, leading to an SEI with desirable mechanical properties that dispersed the stress and restricted crack formation. By contrast, with higher amounts of solventderived components, the SEI formed in BE exhibited lower modulus and uniformity, hence unable to tolerate the volume swing of Si.33 In addition, the observation of microcracks on the electrode surface through SEM agreed with our speculations (Supporting Information Figure S11). The TEM examination results also indicated that the resilient SEI prevented repeated SEI formation. As shown in Figure 3i,j, a thicker SEI was formed in BE compared with that in BE + 1% TVSi. The thick SEI increased the polarization and hindered the migration

of lithium-ion, which explained the electrochemical performance obtained in BE.

Apart from the Si anode, TVSi was also beneficial to the Ni92 cathode. As shown in Figure 4a, the specific capacity retention could be improved from 67% to 83% after 200 cycles with 1% TVSi. Under elevated temperatures, the improvement became more significant (Supporting Information Figure S12): TVSi additive enabled a capacity retention of 77% after 150 cycles at 45 °C while the cell with BE completely failed. Our performance was competitive among currently reported works (Supporting Information Table S1). To reveal the protection mechanism, the mass of the cathodes in both electrolytes was measured in-situ by EQCM. As shown in Figure 4b,c, under high voltages, the mass on the Ni92 cathode was detected to decrease in BE, with a mass variated per mole of electron transferring of –13 g mol⁻¹, higher than that of the delithiation process (-7 g mol⁻¹).³⁴ As the growth of CEI formation resulted in a mass increase, the deviation might be due to the TM (mostly Ni) dissolution in BE. By comparison, in the presence of 1% TVSi, a great mass increment was detected at high voltage, which

DOI: 10.31635/ccschem.024.202404120 **Citation:** *CCS Chem.* **2025**, 7, 429-439



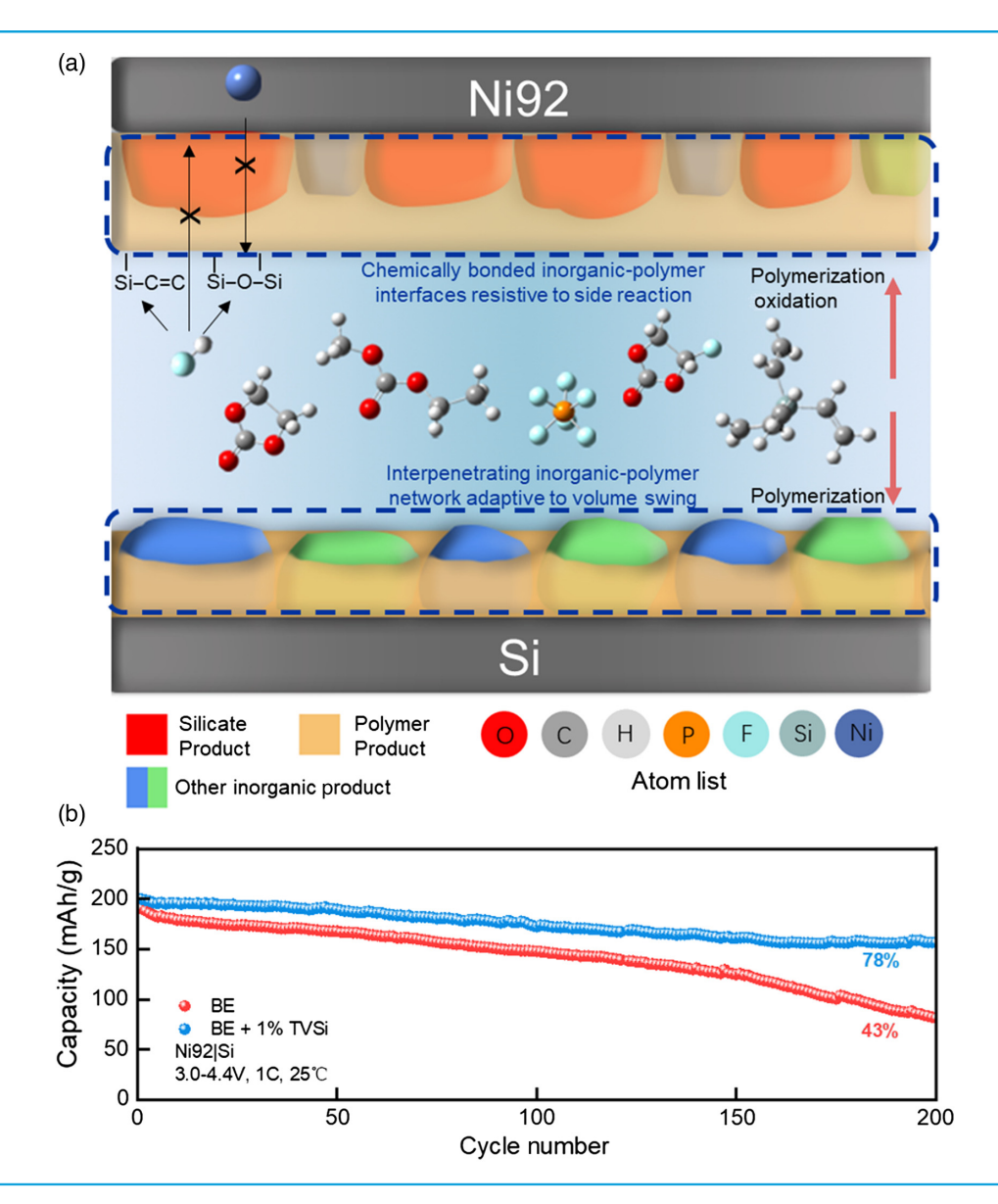


Figure 6 | (a) Schematic illustration of the protective mechanism of TVSi additive. (b) Electrochemical performance of Ni92-Si(prelithiation) full cell.

symbolized additional oxidation progress of TVSi forming a dense CEI to protect the interface. To further observe the Ni dissolution, in-situ UV-vis spectroscopy was utilized to detect the trace TM ion during the cycling (Figure 4d). The peak at ~400 nm, corresponding to Ni²⁺ signal³⁵ was more intense in BE than in BE + 1% TVSi, indicating a more severe Ni dissolution without TVSi. ICP-AES was also applied to measure the TMs deposited on the anode (Figure 4e). The anode cycled with TVSi showed a lower TM content compared with BE, which further confirmed the ability of TVSi suppression in Ni dissolution.

Then XPS was utilized to analyze the components of CEI (Figure 5a-c). Compared with BE, two new peaks at 102.5 and 100.5 eV emerged in the Si2p spectra with 1% TVSi, corresponding to Li-Si-O/Si-F and Si-C respectively. F1s and C1s spectra also confirmed the existence of

Si-F and Si-C bonding. The existence of Si-C and Si-O bonds originated mostly from the products of TVSi and the Si-F bond, possibly related to the HF scavenging process. TOFSIMS measurement was performed to further analyze the possible product (Figure 5d, Supporting Information Figures S13 and S14). According to the threedimensional (3D) distribution graphs and fragments distribution curve, a wealth of fluorinated fragments such as SiF_3^- , $SiF_4^-SiO_2F_2^-$, and $C_2H_3SiF_2^-$ were observed on the surface. These fragments were probably the result of the reaction between silicate (or TVSi) and HF. To verify the mechanism of the HF scavenging process, DFT calculation was applied to investigate the reaction process (Figure 5e,f). HF could be eliminated by a reaction with TVSi or (Si-C=C group) via Si-C breaking and Si-F formation with an electron loss. The transition state of the reaction was 0.76 eV higher than the reactant and the

DOI: 10.31635/ccschem.024.202404120 **Citation:** *CCS Chem.* **2025**, 7, 429-439



energy level of the final product was lower than the reactant, demonstrating the feasibility of the reaction. The silicate in the CEI also played a role in scavenging the HF. The oxygen was initially coordinated with hydrogen to form a hydroxyl group. The hydroxyl group later reacted with HF via a Si-O breaking and Si-F formation. Therefore, during the charge-discharge process, when HF was transferring to the Ni92 cathode, the CEI captured it before it came in contact with the surface lattice, restraining its attack on the Ni92 phase and suppressing the nickel dissolution. By scavenging the HF, the severe crack formation in secondary particles was also inhibited. As shown in Supporting Information Figure S15, severe cracks were formed in BE, which further increased the electrolyte contact areas, and thus, accelerated the electrolyte consumption and structural damage of Ni92.

According to the distribution curves of TOFSIMs, in addition to commonly reported inorganic fragments such as LiF2-, inorganic fragments originating from silicate such as LiSiO₃⁻ and LiSiO₄⁻ were detected concentrating on the top of CEI. The above results suggested that TVSi initially formed a silane polymer layer on the cathode, which later, partially oxidized on the cathode surface to form inorganic-silane composite CEI products with chemically bonded interfaces, resulting in enhanced rigidity and mechanical strength (Supporting Information Figure S16). This compact CEI structure served as a barrier, preventing penetration of the electrolyte, thereby reducing the probability of side reactions. Furthermore, the silicate contacting the cathode phase played an important role in restraining the side reactions. The much stronger bonding energy of Si-O (798 kJ/mol) than TM-O (391.6 kJ/mol) dragged the oxygen atoms toward Si atoms from Ni atoms, reducing the nickel oxidation valence state.³⁶ As mostly reported, higher Ni valence had a higher catalytic activity that induced serious side reactions, which not only led to the consumption of the electrolyte but also accelerated the cation mixing causing an irreversible phase transition.³⁷⁻³⁹ Therefore, the compact and functional CEI was expected to restrain the rock-salt phase transition. TEM results (Supporting Information Figure S17) also showed that for the Ni92 cathode cycled in BE, a large rock-salt phase region was observed, which was not only electrochemically inert but also obstructive to lithium-ion transfer. By sharp contrast, the rock-salt phase could be barely observed in the material cycled in BE + 1% TVSi.

From the experimental and theoretical results, the function of TVSi is schematically illustrated in Figure 6a. TVSi polymerized on the electrode and mechanically bonded with inorganic components to form a resilient composite SEI, which was capable of accommodating volume changes of Si, suppressing constant electrolyte consumption and SEI growth. At the cathode, when HF was attacking the lattice, the Si-C=C and

Si-O functional structure on the surface of the cathode could pre-emptively react with it, thereby restricting the Ni dissolution. Additionally, the chemical bonding between inorganic-organic interfaces within CEI inhibited the penetration of the electrolyte, thus reducing the side reactions and hampering the irreversible phase transition. Finally, proof-of-concept full cells consisting of Ni92 cathode and prelithiated Si anode were assembled and tested. As shown in Figure 6b and Supporting Information Figure S18, the specific capacity retention of the full cells greatly improved at both 25 and 45 °C, demonstrating large potentials of TVSi in practical use.

Conclusion

This work presented a comprehensive investigation into the capacity of TVSi as an electrolyte additive in lithiumion batteries, with a particular focus on Si anodes and Nirich cathodes. The integration of TVSi significantly bolstered battery stability and performance. In Si anodes, TVSi enabled the formation of an interpenetrating network composite SEI consisting of flexible silane-based polymer embedded with rigid inorganic components. This SEI adeptly accommodated the volume swing of Si, thereby reducing electrolyte consumption and SEI aging. On the cathode side, TVSi contributed to the formation of an inorganic-silane composite CEI with chemically bonded interfaces. The dense CEI not only curtailed the nickel dissolution but also impeded the electrolyte penetration inhibited the side reaction, and further suppressed the irreversible phase transition. Consequently, the dual functionality of TVSi in stabilizing both electrodes led to notable improvement of the full cell. This research paves the way for the development of electrolyte additives, capable of constructing tailored SEI and CEI to further advance battery design.

Supporting Information

Supporting Information is available and includes supplementary data of this manuscript.

Conflict of Interest

There is no conflict of interest to report.

Funding Information

This work was supported by the National Natural Science Foundation of China (NSFC; grant no. 52303263), the Shenzhen Science and Technology Research Grants, China (grant no. JCYJ20200109140416788), and the Soft Science Research Project of Guangdong Province, China (grant no. 2017B030301013).

DOI: 10.31635/ccschem.024.202404120 **Citation:** *CCS Chem.* **2025**, 7, 429-439



References

- 1. Guo, J.; Dong, D.; Wang, J.; Liu, D.; Yu, X.; Zheng, Y.; Wen, Z.; Lei, W.; Deng, Y.; Wang, J.; Hong, G.; Shao, H. Silicon-Based Lithium Ion Battery Systems: State-of-the-Art from Half and Full Cell Viewpoint. *Adv. Funct. Mater.* **2021**, *31*, 2102546.
- 2. Ge, M.; Cao, C.; Biesold, G. M.; Sewell, C. D.; Hao, S.-M.; Huang, J.; Zhang, W.; Lai, Y.; Lin, Z. Recent Advances in Silicon-Based Electrodes: From Fundamental Research Toward Practical Applications. *Adv. Mater.* **2021**, *33*, 2004577.
- 3. Ryu, H.-H.; Park, K.-J.; Yoon, C. S.; Sun, Y.-K. Capacity Fading of Ni-Rich Li[Ni $_x$ Co $_y$ Mn $_{1-x-y}$]O $_2$ (0.6 \le x \le 0.95) Cathodes for High-Energy-Density Lithium-Ion Batteries: Bulk or Surface Degradation? *Chem. Mater.* **2018**, *30*, 1155-1163.
- 4. Li, W.; Erickson, E. M.; Manthiram, A. High-Nickel Layered Oxide Cathodes for Lithium-Based Automotive Batteries. *Nat. Energy* **2020**, *5*, 26–34.
- 5. Wu, H.; Cui, Y. Designing Nanostructured Si Anodes for High Energy Lithium Ion Batteries. *Nano Today* **2012**, *7*, 414-429.
- 6. Qian, G.; Li, Y.; Chen, H.; Xie, L.; Liu, T.; Yang, N.; Song, Y.; Lin, C.; Cheng, J.; Nakashima, N.; Zhang, M.; Li, Z.; Zhao, W.; Yang, X.; Lin, H.; Lu, X.; Yang, L.; Li, H.; Amine, K.; Chen, L.; Pan, F. Revealing the Aging Process of Solid Electrolyte Interphase on SiOx Anode. *Nat. Commun.* **2023**, *14*, 6048.
- 7. Jin, Y.; Zhu, B.; Lu, Z.; Liu, N.; Zhu, J. Challenges and Recent Progress in the Development of Si Anodes for Lithium-lon Battery. *Adv. Energy Mater.* **2017**, *7*, 1700715.
- 8. Etacheri, V.; Haik, O.; Goffer, Y.; Roberts, G. A.; Stefan, I. C.; Fasching, R.; Aurbach, D. Effect of Fluoroethylene Carbonate (FEC) on the Performance and Surface Chemistry of Si-Nanowire Li-Ion Battery Anodes. *Langmuir* **2012**, *28*, 965–976.
- 9. Markevich, E.; Salitra, G.; Aurbach, D. Fluoroethylene Carbonate as an Important Component for the Formation of an Effective Solid Electrolyte Interphase on Anodes and Cathodes for Advanced Li-lon Batteries. *ACS Energy Lett.* **2017**, *2*, 1337–1345.
- 10. Xu, C.; Lindgren, F.; Philippe, B.; Gorgoi, M.; Björefors, F.; Edström, K.; Gustafsson, T. Improved Performance of the Silicon Anode for Li-Ion Batteries: Understanding the Surface Modification Mechanism of Fluoroethylene Carbonate as an Effective Electrolyte Additive. *Chem. Mater.* **2015**, *27*, 2591-2599.
- 11. Zhu, C.; Chen, S.; Li, K.; Yin, Z.-W.; Xiao, Y.; Lin, H.; Pan, F.; Yang, L. Quantitative Analysis of the Structural Evolution in Si Anode via Multi-Scale Image Reconstruction. *Sci. Bull.* **2023**, *68*, 408–416.
- 12. Chen, J.; Fan, X.; Li, Q.; Yang, H.; Khoshi, M. R.; Xu, Y.; Hwang, S.; Chen, L.; Ji, X.; Yang, C.; He, H.; Wang, C.; Garfunkel, E.; Su, D.; Borodin, O.; Wang, C. Electrolyte Design for LiF-Rich Solid-Electrolyte Interfaces to Enable High-Performance Microsized Alloy Anodes for Batteries. *Nat. Energy* **2020**, *5*, 386–397.
- 13. Cao, Z.; Zheng, X.; Qu, Q.; Huang, Y.; Zheng, H. Electrolyte Design Enabling a High-Safety and High-Performance Si

- Anode with a Tailored Electrode-Electrolyte Interphase. *Adv. Mater.* **2021**, *33*, 2103178.
- 14. Rinkel, B. L. D.; Hall, D. S.; Temprano, I.; Grey, C. P. Electrolyte Oxidation Pathways in Lithium-Ion Batteries. *J. Am. Chem. Soc.* **2020**, *142*, 15058–15074.
- 15. Jayawardana, C.; Rodrigo, N.; Parimalam, B.; Lucht, B. L. Role of Electrolyte Oxidation and Difluorophosphoric Acid Generation in Crossover and Capacity Fade in Lithium Ion Batteries. *ACS Energy Lett.* **2021**, *6*, 3788–3792.
- 16. Kim, K.; Park, I.; Ha, S.-Y.; Kim, Y.; Woo, M.-H.; Jeong, M.-H.; Shin, W. C.; Ue, M.; Hong, S. Y.; Choi, N.-S. Understanding the Thermal Instability of Fluoroethylene Carbonate in LiPF₆-Based Electrolytes for Lithium Ion Batteries. *Electrochim. Acta* **2017**, *225*, 358–368.
- 17. Zhao, X.; Zhuang, Q.-C.; Xu, S.-D.; Xu, Y.-X.; Shi, Y.-L.; Zhang, X.-X. A New Insight into the Content Effect of Fluoroethylene Carbonate as a Film Forming Additive for Lithium-Ion Batteries. *Int. J. Electrochem. Sci.* **2015**, *10*, 2515–2534.
- 18. Sahore, R.; O'Hanlon, D. C.; Tornheim, A.; Lee, C.-W.; Garcia, J. C.; Iddir, H.; Balasubramanian, M.; Bloom, I. Revisiting the Mechanism Behind Transition-Metal Dissolution from Delithiated LiNi $_x$ Mn $_y$ Co $_z$ O $_2$ (NMC) Cathodes. *J. Electrochem. Soc.* **2020**, *167*, 020513.
- 19. Zhang, D.; Liu, M.; Ma, J.; Yang, K.; Chen, Z.; Li, K.; Zhang, C.; Wei, Y.; Zhou, M.; Wang, P.; He, Y.; Lv, W.; Yang, Q.-H.; Kang, F.; He, Y.-B. Lithium Hexamethyldisilazide as Electrolyte Additive for Efficient Cycling of High-Voltage Non-Aqueous Lithium Metal Batteries. *Nat. Commun.* **2022**, *13*, 6966.
- 20. Chen, Z.; Soltani, A.; Chen, Y.; Zhang, Q.; Davoodi, A.; Hosseinpour, S.; Peukert, W.; Liu, W. Emerging Organic Surface Chemistry for Si Anodes in Lithium-Ion Batteries: Advances, Prospects, and Beyond. *Adv. Energy Mater.* **2022**, *12*, 2200924.
- 21. Fang, J.-B.; Chang, S.-Z.; Ren, Q.; Zi, T.-Q.; Wu, D.; Li, A.-D. Tailoring Stress and Ion-Transport Kinetics via a Molecular Layer Deposition-Induced Artificial Solid Electrolyte Interphase for Durable Silicon Composite Anodes. *ACS Appl. Mater. Interfaces* **2021**, *13*, 32520–32530.
- 22. Wang, H.; Sun, D.; Li, X.; Ge, W.; Deng, B.; Qu, M.; Peng, G. Alternative Multifunctional Cyclic Organosilicon as an Efficient Electrolyte Additive for High Performance Lithium-Ion Batteries. *Electrochim. Acta* **2017**, *254*, 112–122.
- 23. Dong, Z.; Wei, J.; Yue, H.; Zhang, K.; Wang, L.; Li, X.; Zhang, Z.; Yang, W.; Yang, S. Multifunctional Organosilicon Compound Contributes to Stable Operation of High-Voltage Lithium Metal Batteries. *J. Colloid Interface Sci.* **2021**, *595*, 35–42.
- 24. Han, J.-G.; Jeong, M.-Y.; Kim, K.; Park, C.; Sung, C. H.; Bak, D. W.; Kim, K. H.; Jeong, K.-M.; Choi, N.-S. An Electrolyte Additive Capable of Scavenging HF and PF $_5$ Enables Fast Charging of Lithium-Ion Batteries in LiPF $_6$ -Based Electrolytes. *J. Power Sources* **2020**, *446*, 227366.
- 25. Haridas, A. K.; Nguyen, Q. A.; Terlier, T.; Blaser, R.; Biswal, S. L. Investigating the Compatibility of TTMSP and FEC Electrolyte Additives for LiNi_{0.5}Mn_{0.3}Co_{0.2}O₂ (NMC)-Silicon Lithium-Ion Batteries. *ACS Appl. Mater. Interfaces* **2021**, *13*, 2662–2673.

DOI: 10.31635/ccschem.024.202404120 **Citation:** *CCS Chem.* **2025**, 7, 429-439



- 26. Zhang, Y.; Katayama, Y.; Tatara, R.; Giordano, L.; Yu, Y.; Fraggedakis, D.; Sun, J. G.; Maglia, F.; Jung, R.; Bazant, M. Z.; Shao-Horn, Y. Revealing Electrolyte Oxidation via Carbonate Dehydrogenation on Ni-Based Oxides in Li-lon Batteries by In Situ Fourier Transform Infrared Spectroscopy. *Energy Environ. Sci.* **2020**, *13*, 183–199.
- 27. Yan, Y.; Weng, S.; Fu, A.; Zhang, H.; Chen, J.; Zheng, Q.; Zhang, B.; Zhou, S.; Yan, H.; Wang, C.-W.; Tang, Y.; Luo, H.; Mao, B.-W.; Zheng, J.; Wang, X.; Qiao, Y.; Yang, Y.; Sun, S.-G. Tailoring Electrolyte Dehydrogenation with Trace Additives: Stabilizing the LiCoO₂ Cathode Beyond 4.6 V. *ACS Energy Lett.* **2022**, *7*, 2677–2684.
- 28. Ji, Y.; Qiu, J.; Zhao, W.; Liu, T.; Dong, Z.; Yang, K.; Zheng, G.; Qian, G.; Yang, M.; Chen, Q.; Amine, K.; Pan, F.; Yang, L. In Situ Probing the Origin of Interfacial Instability of Na Metal Anode. *Chem* **2023**, *9*, 2943–2955.
- 29. Sun, C.; Wang, Y.-J.; Gu, H.; Fan, H.; Yang, G.; Ignaszak, A.; Tang, X.; Liu, D.; Zhang, J. Interfacial Coupled Design of Epitaxial Graphene@SiC Schottky Junction with Built-In Electric Field for High-Performance Anodes of Lithium Ion Batteries. *Nano Energy* **2020**, *77*, 105092.
- 30. Huang, D.; Yin, L.; Niu, J. Photoinduced Hydrodefluorination Mechanisms of Perfluorooctanoic Acid by the SiC/Graphene Catalyst. *Environ. Sci. Technol.* **2016**, *50*, 5857-5863.
- 31. Brunet, M.; Aureau, D.; Chantraine, P.; Guillemot, F.; Etcheberry, A.; Gouget-Laemmel, A. C.; Ozanam, F. Etching and Chemical Control of the Silicon Nitride Surface. *ACS Appl. Mater. Interfaces* **2017**, *9*, 3075–3084.
- 32. Aupperle, F.; Eshetu, G. G.; Eberman, K. W.; Xioa, A.; Bridel, J.-S.; Figgemeier, E. Realizing a High-Performance LiNi_{0.6}Mn_{0.2}Co_{0.2}O₂/Silicon-Graphite Full Lithium Ion

- Battery Cell via a Designer Electrolyte Additive. *J. Mater. Chem. A* **2020**, *8*, 19573–19587.
- 33. Zhao, Q.; Stalin, S.; Archer, L. A. Stabilizing Metal Battery Anodes Through the Design of Solid Electrolyte Interphases. *Joule* **2021**, *5*, 1119–1142.
- 34. Ji, Y.; Yin, Z.-W.; Yang, Z.; Deng, Y.-P.; Chen, H.; Lin, C.; Yang, L.; Yang, K.; Zhang, M.; Xiao, Q.; Li, J.-T.; Chen, Z.; Sun, S.-G.; Pan, F. From Bulk to Interface: Electrochemical Phenomena and Mechanism Studies in Batteries via Electrochemical Quartz Crystal Microbalance. *Chem. Soc. Rev.* **2021**, *50*, 10743–10763.
- 35. Jin, B.; Cui, Z.; Manthiram, A. In Situ Interweaved Binder Framework Mitigating the Structural and Interphasial Degradations of High-Nickel Cathodes in Lithium-Ion Batteries. *Angew. Chem. Int. Ed.* **2023**, *62*, e202301241.
- 36. Jiang, Y.; Bi, Y.; Liu, M.; Peng, Z.; Huai, L.; Dong, P.; Duan, J.; Chen, Z.; Li, X.; Wang, D.; Zhang, Y. Improved Stability of Ni-Rich Cathode by the Substitutive Cations with Stronger Bonds. *Electrochim. Acta* **2018**, *268*, 41–48.
- 37. Jiang, M.; Danilov, D. L.; Eichel, R.-A.; Notten, P. H. L. A Review of Degradation Mechanisms and Recent Achievements for Ni-Rich Cathode-Based Li-Ion Batteries. *Adv. Energy Mater.* **2021**, *11*, 2103005.
- 38. Kim, U.-H.; Ryu, H.-H.; Kim, J.-H.; Mücke, R.; Kaghazchi, P.; Yoon, C. S.; Sun, Y.-K. Microstructure-Controlled Ni-Rich Cathode Material by Microscale Compositional Partition for Next-Generation Electric Vehicles. *Adv. Energy Mater.* **2019**, 9, 1803902.
- 39. Park, N.-Y.; Park, G.-T.; Kim, S.-B.; Jung, W.; Park, B.-C.; Sun, Y.-K. Degradation Mechanism of Ni-Rich Cathode Materials: Focusing on Particle Interior. *ACS Energy Lett.* **2022**, *7*, 2362–2369.

DOI: 10.31635/ccschem.024.202404120 **Citation:** *CCS Chem.* **2025**, 7, 429-439